Installation of New Electron Cyclotron Emission Imaging in LHD*)

Hayato TSUCHIYA[1)], Daisuke KUWAHARA[2)], Tokihiko TOKUZAWA[1)], Yoshio NAGAYAMA[3)], Yuki TAKEMURA[1,4)] and LHD Experiment Group

[1)]*National Institute for Fusion Science, Toki, Gifu 509-5292, Japan*
[2)]*Tokyo University of Agriculture and Technology, Tokyo 184-8588, Japan*
[3)]*Nihon University, Tokyo 101-8308, Japan*
[4)]*SOKENDAI (The Graduate University for Advanced Studies), Toki 509-5292, Japan*

(Received 28 December 2017 / Accepted 15 March 2018)

A new electron cyclotron emission imaging antenna was designed and installed outside the torus on LHD. To improve the signal quality, we developed a local oscillator integrated antenna array (LIA), in which each channel has an internal local oscillation supply from a frequency-multiplier-integrated circuit. The labyrinth structure of the optical system comprises five mirrors to protect the LIA from plasma neutron emission. The initial results were obtained from the 2017 LHD experimental campaign. The MHD fluctuations and their fluctuation profiles were observed.

Keywords: ECEI, LHD, multi horn antenna array, microwave optics

DOI: 10.1585/pfr.13.3402063

1. Introduction

Millimeter-wave-imaging systems have been employed in large-scale plasma devices. Electron cyclotron emission imaging (ECEI) is recognized to be one of the valuable tools because ECEI diagnostics are expected for the measurement of micro turbulence as well as well-known MHD fluctuations that can be often observed by conventional ECE [1]. The ECEI system was developed by the UC Davis group [2, 3] and has been installed in tokamaks and other devices [3–7].

A microwave-imaging reflectometer was employed with ECEI on LHD until 2016 [8–14]. At the beginning of the D-D plasma experiment of LHD, we refined the receiving antennas called as Horn-antenna Millimeter Imaging Device (HMID) [13], which was originally developed by the LHD group. By improving the internal LO supply using a frequency-multiplier-integrated circuit in each channel, a 40 dB gain increase is expected [10]. The new antenna was named as the new local integrated antenna array (LIA). The installed optical system and the initial ECEI results are described in this manuscript.

2. ECEI Optics on LHD

The line of sight is on the mid plane of the horizontally-elongated-magnetic-field cross section (4-O port). A conventional ECE antenna was also installed near the opposite torus section of LHD [1]. In conventional ECE systems (1D-ECE), the millimeter wave of the ECE can easily transmit by corrugated waveguides and can be detected by the heterodyne detector with a filter bank system outside the torus hall. In the case of the ECEI system, it is necessary to detect the ECE in the torus hall using imaging detectors.

Figure 1 shows the layout of the ECEI optical system on LHD and the beam path. The focus on the plasma is located near the half-radius point to detect the oscillation on the $\iota = 1$ ($m/n = 1/1$) surface. The ECEI rack that contains the LIA should be at a distance from the LHD outer vacuum vessel to protect the semiconductors in the LIA from fast neutrons. At 5 m from LHD, the majority of the fast neutrons are moderated and the thermal neutrons dominate. To reduce the effect of thermal neutrons, the ECEI rack is shielded by a 5-cm-thick polyethylene wall. The DC-power supply of LIA and IF-amplifier are located in another rack with a 10-cm-thick polyethylene shield to reduce risk.

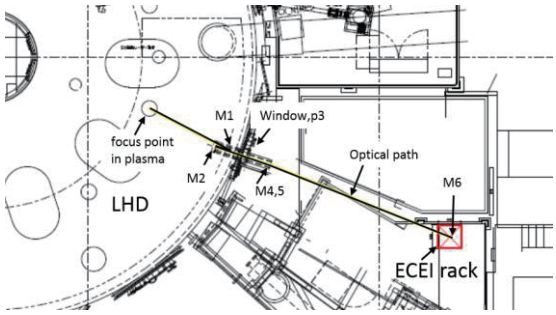

Fig. 1 Layout of the ECEI optical system. This image is a top view of LHD and the diagnostic stage. Mirrors are indicated as M1, M2, M4, M5, and M6 on the optical path, and P3 is the vacuum window.

author's e-mail: tsuchiya.hayato@nifs.ac.jp

*) This article is based on the presentation at the 26th International Toki Conference (ITC26).

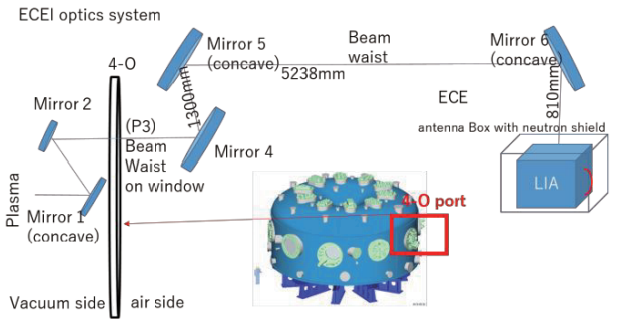

Fig. 2 Conceptual diagram of the ECEI optical system (side view).

Between the plasma focus point and the LIA, the optical system comprises concaved mirrors (M1, M5, M6), plane mirrors (M2, M4), and a window (P3). The optical path is on a different plane to maintain a clearance from neighboring devices. The ECEI rack of M6 and the LIA is separated from the LHD port that mirrors (M1, M2, M4, and M5) are attached. The fine adjustment mechanisms are provided on M5 and M6 to tune the beam path. The mirrors must be large enough to cover the expanded beam since the millimeter wave of ECE propagates as a Gaussian beam in the free space. Figure 2 shows the side-view conceptual diagram of the optical system. The mirror size and optical path length are restricted by the matching conditions of the Gaussian beam and the effective radius of the vacuum window. Both mirrors are concaved to match the Gaussian beam between M5 and M6, which are designed by the concept of a constant-phase mirror in the following equation [1, 15]:

$$\Psi_{\mathrm{in}}(\mathbf{r}) + \Psi_{\mathrm{out}}(\mathbf{r}) = \text{constant}, \tag{1}$$

where $\Psi_{\mathrm{in}}(\mathbf{r})$ and $\Psi_{\mathrm{out}}(\mathbf{r})$ are the input and desired output Gaussian beam phase from the focus point at mirror surface position $\boldsymbol{r}$, respectively. The constant-phase mirror enables the shape of the Gaussian beam to be controlled. We assume that the dominant radiation pattern is Gaussian-type from each horn antenna of the LIA. The spot size at the LIA is designed to correspond to the size of each horn antenna aperture of LIA (~ 14 mm radius). The restricted condition is the size of window (25 mm radius). Figure 3 shows the development of the designed beam radius and the measured beam size propagation. Since the measured ECE frequency is greater than 50 GHz, we designed mirrors optimized at 50 GHz. The diameters of M4, M5, and M6 are 200 mm to cover 1.5σ of the spreading beam. Figure 3 (b) shows the result of the beam propagation test in the air. The test beam is radiated from P3 using a horn antenna with a 40-mm × 30-mm aperture. The beam size and beam profile are measured at the LIA position. Figure 3 (b) shows the measured beam size and calculated ideal beam propagation of 54 GHz near the beam waist position. The horizontal axis is the light path from M6 in Fig.3 (a). The 810 mm position corresponds to the right end of Fig.3 (a).

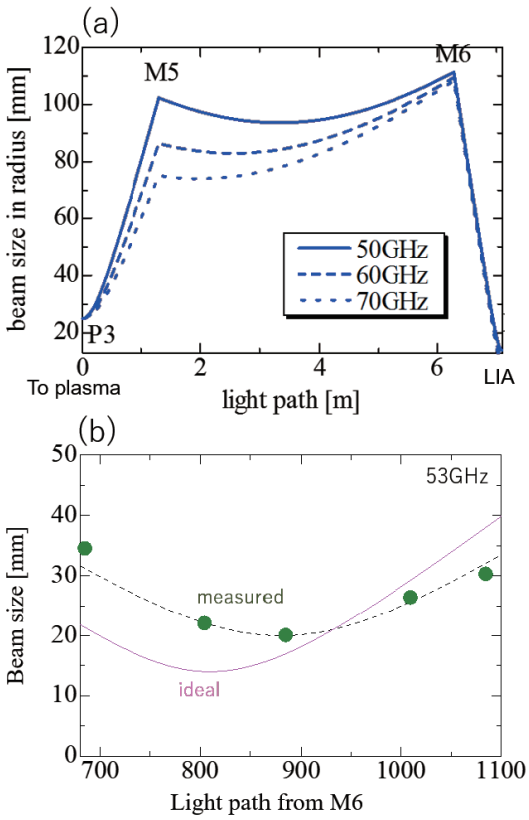

Fig. 3 (a) The development of the designed beam radius from vacuum window (P3) to LIA. (b) The comparison of beam size between designed size and measured size. The RF frequency is 53 GHz.

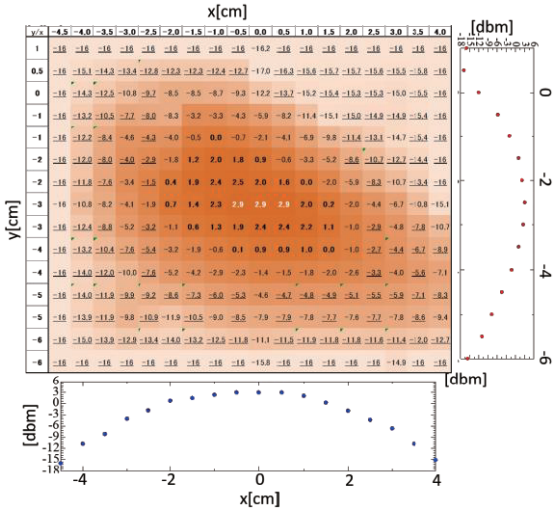

Fig. 4 Measured beam pattern at the beam-waist position [x = 885 mm in Fig. 3 (b)]. The probe Gaussian beam is radiated from P3 to LIA. The RF frequency is 53 GHz.

The designed beam waist is at 800 mm and 14 mm in size, with a 25 mm beam waist size at P3. The measured beam waist radius is ~ 30 mm because the measured beam waist size at P3 is not exactly the same as the ideal size. However, the focal length is considered not to be different in terms of size. Figure 4 shows the measured beam pattern

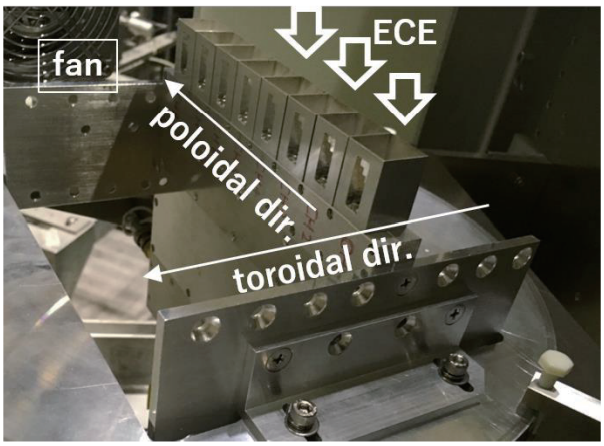

Fig. 5 Image of the installed LIA on LHD.

at the beam waist position. Although the beam pattern has a slightly oblong shape, the matching to the LIA is acceptable. Based on this result, the LIA is installed at the measured waist position when the optical system is installed to LHD.

3. View Area on LHD

An 8-ch array of LIA is adopted on ECEI of LHD. The working frequency band of the LIA is 50 - 60 GHz. An ECE wave at a frequency in the range of 50 - 57 GHz is obtained by each horn antenna of the LIA and down-converted by each channel array of the LIA. The down-converted intermediate frequency (IF) signals are separated and detected by the filter bank. The frequency resolution is $\Delta f = 1$ GHz, and the observed frequencies of each channel are integers from 50 to 57 GHz, with eight channels in total. The detailed technical information regarding the LIA was described previously [14].

The image of installed LIA is shown in Fig. 5. The direction of the horn antenna array is placed in a parallel direction to the poloidal direction. This setting is used for measuring the poloidal-radial cross section. In the 2017 LHD experimental campaign, a system with 8-ch in radial was used. There is one LIA unit in the images, but another LIA unit can be installed beside the LIA, and the LIA is a compact system. By using several LIA units, the ECEI can be expanded to become a poloidal-radial-toroidal 3D-imaging system.

Figure 6 shows the field of view of ECEI at a LHD typical magnetic field configuration. The maximum magnetic field strength of LHD is approximately 3 T. The ECEI system was designed for the half-magnetic-field configuration to detect electron temperature fluctuations driven by MHD instability. At 1.375 T, the rational surface (m/n = 1/1) is within the ECEI field of view. Inside the last closed flux surface, the optical depth of the X-mode 2nd harmonics is more than 10. At the case of 1.5 T, a part of observation volume (i.e., observation region of low frequency

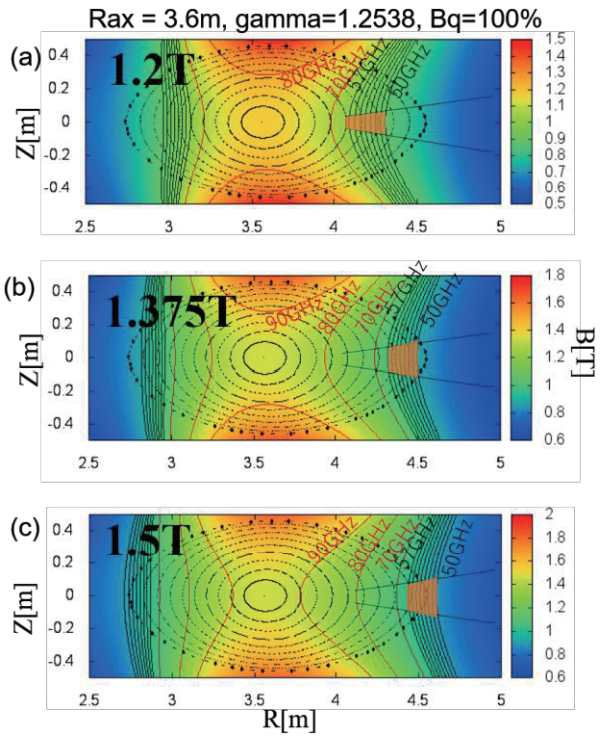

Fig. 6 Typical field-of-view of ECEI. The magnetics are in the standard configuration as follows: Magnetic axis (R_{ax}) is 3.6 m. The pitch parameter (γ) is 1.2538. The quadrupole field component (B_q) is 100%. The magnetic field strengths are (a) 1.2 T, (b) 1.375 T, (c) 1.5 T. The color scale shows the profile of magnetic field strength. The dot is the Poincare plot of closed flux surface. The solid line with label is the 2nd harmonics of electron cyclotron resonance of each frequency. The colored region is field of view of 8-ch × 8-ch ECEI.

channels) are outside the last closed flux surface. Because the density is not high enough in the ergodic region, we must consider the effect of the optical depth of gray [16].

4. Initial Result on LHD

The installed ECEI system has been successfully operated since the 2017 LHD experimental campaign. The time-series data of 64 channels are simultaneously acquired by a PXI (National Instruments) module. Typical sampling rate is 1 MS/s and the data length is 10 s, which covers the discharge duration time of a standard LHD experiment. In long-pulse-discharge experiments, continuous data acquisition is enabled by the reducing the sampling rate to 100 kS/s.

Figure 7 shows the electron temperature profile derived from DC components of RF. Because each channel has not been absolutely calibrated, the calibration is conducted by fitting the electron temperature profile data that is observed by Thomson scattering at the steady-state plasma. The view area in Fig. 7 corresponds to the area shown in Fig. 6 (b). The plasma of Fig. 7 is superimposed on the power modulation electron cyclotron heat-

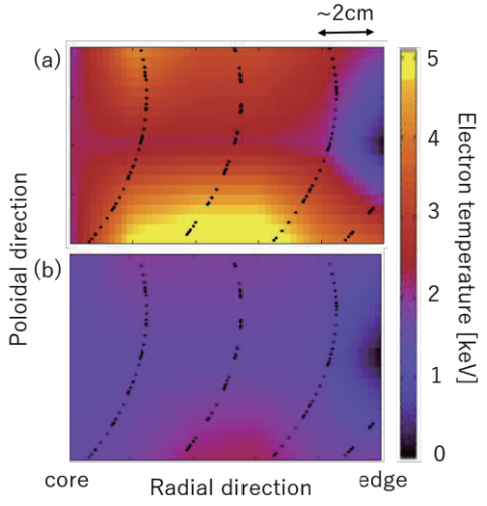

Fig. 7 The electron temperature profile during modulation electron cyclotron heating. (a) Profile for ECH on. (b) Profile for ECH off. The color bars indicate the electron temperature in keV. The black dots are the Poincare plots of closed flux surface.

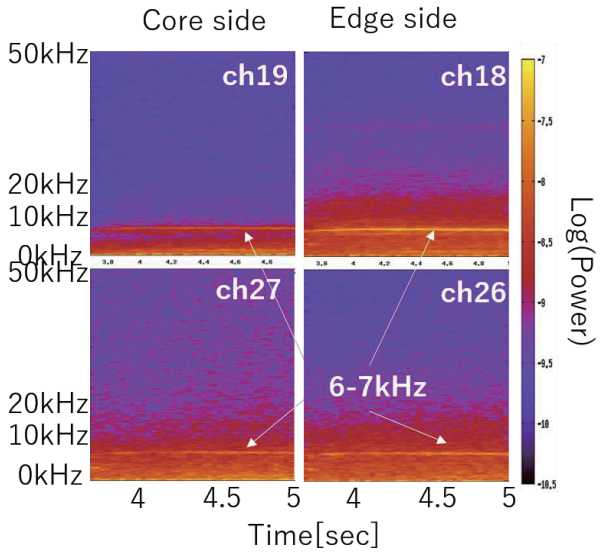

Fig. 8 Development of the power spectrum of the electron temperature. The left column (ch-19,27) are the spectra of f_{ece} = 52 GHz. The right column (ch-18,26) is spectra of f_{ece} = 51 GHz. Ch-18 and 19 are derived from the same horn antenna of the LIA.

ing. The profiles were recorded just after the injection of ECH, and without the injection of ECH. Clearly, the high-temperature region on the core side is generated. The flux surface lies vertically in Fig. 7, but it does not appear to be the same temperature on the surface.

Figure 8 shows the Fourier analysis result of electron temperature fluctuations, which were strongly observed in the core side of the field of view in Fig. 6 (b). The power peak of 6 - 7 kHz fluctuations was observed by all channels. They were found to be the m/n = 1/1 MHD instability around ι = 1 surface. The fluctuations have strong coherence with magnetic oscillations, and with each other in ECEI channels. The fluctuation phase was also calculated, and the propagation and the correlation length can be estimated. The fluctuation was also detected by a conventional 1D-ECE measurement. The mode-profile peak observed by ECEI and 1D-ECE are different. This indicates that there is alignment inexactness or beam bending of ECEI. Since the sight line of ECEI is not exactly along the radial direction, the beam may bend toward the tangential direction by the plasma on the complex shaped ergodic layer.

5. Summary and Future Plan

ECEI optics was designed and installed outside of the torus on LHD. An 8ch LIA of V-band is employed as imaging antenna. Since the 2017 LHD experimental campaign, the ECEI system has provided the relative 2D electron temperature profile and its fluctuation. To provide the absolute temperature profile, the LIA gain will be calibrated using a hot source and the ray trace simulation with LHD plasma should be necessary. LIA units will be installed to expand ECEI from 2D-diagnostic to 3D-diagnostic. The LIA high frequency band will also be ready for the standard higher magnetic field configuration experiment.

Acknowledgments

This work was performed with the support of the NIFS budget (NIFS17ULPP008, NIFS17ULPP020) and NIFS Collaborative Research Program (NIFS15KOAP029).

[1] H. Tsuchiya *et al*, Plasma Fusion Res. **6**, 2402114 (2011).
[2] H. Park *et al.*, Rev. Sci. Instrum. **75**, 3875 (2004).
[3] B. Tobias *et al.*, Rev. Sci. Instrum. **81**, 10D928 (2010).
[4] G.S. Yun *et al.*, Rev. Sci. Instrum. **85**, 11D820 (2014).
[5] C. Luo *et al.*, J. Instrum. **9**, P12014 (2014).
[6] B.H. Deng *et al.*, Rev. Sci. Instrum. **72**, 301 (2001).
[7] B.H. Deng *et al.*, Rev. Sci. Instrum. **70**, 998 (1999).
[8] Y. Nagayama *et al.*, Plasma Fusion Res. **11**, 2402111 (2016).
[9] Y. Nagayama *et al.*, Rev. Sci. Instrum. **88**, 044703 (2017).
[10] D. Kuwahara *et al.*, J. Plasma Fusion Res. **8**, 649 (2009).
[11] A. Mase, Fusion Eng. Des. **53**, 87 (2001).
[12] Y. Kogi, Plasma Fusion Res. **2**, S1032 (2007).
[13] D. Kuwahara *et al.*, Rev. Sci. Insturm. **81** 10D919 (2010).
[14] D. Kuwahara *et al.*, J. Instrum. **10**, C12031 (2015).
[15] S. Kubo *et al.*, Fusion Eng. Des. **26**, 319 (1995).
[16] J. Lee *et al.*, Phys. Rev. Lett. **117**, 075001 (2016).